

Compressive quantum waveform estimation

Alex Tritt,^{1,*} Joshua Morris,^{1,†} Christopher C. Bounds,¹
Hamish A. M. Taylor,¹ James Saunderson,² and L. D. Turner¹

¹*School of Physics & Astronomy, Monash University, Victoria 3800, Australia.*

²*Department of Electrical and Computer Systems Engineering, Monash University, Victoria 3800, Australia.*

Applying quantum sensors to sample entire signals (quantum waveform estimation) promises to revolutionize the sensing of small signals, such as the monitoring of electrical pulses generated by neurons for medical research. However, intensive use of quantum resources (*e.g.*, long sensing times and/or many destructive measurements) make current implementations impractical for real-world use. In this Letter, we experimentally demonstrate quantum waveform estimation of a synthesized neural-like signal, taking many fewer cold-atom measurements than would naively be necessary.

Quantum waveform estimation extends the applicability of precise quantum sensors to the realm of sampling entire signals [1], at the cost of requiring many quantum measurements. One proposed application is the non-invasive sensing of electrical communication in a network of neurons by recording proximal magnetic fields [2–9]. Such measurements would aid in understanding the brain on the microscale, in health and in disease [10]. Neural waveforms, composed of bipolar pulses separated by large gaps [11], clearly contain scant information: sampling one uniformly at its Nyquist rate [12, Sec. 7.1] will measure mostly silence. If information is so sparse, then could one save on resources by taking far fewer quantum measurements? Naively reducing a uniform sample rate, however, would ultimately lose pulses to aliasing. In this Letter, we use compressive sensing to demonstrate quantum waveform estimation of a sparse, neural-like magnetic signal using many fewer quantum measurements than the Nyquist-Shannon sampling theorem would deem necessary.

The modern mathematics of compressive sensing [13–15] (also *compressed sensing* or *compressive sampling*) describes how, under certain conditions, sparse signals can be fully recovered from an *incomplete* set of measurements. Compressive sensors thrive where there is benefit to taking few measurements, *e.g.*, cameras for wavelengths with expensive photodetectors [16], and computed tomography scans which irradiate patients [17]. Compressive sensing in quantum science has assisted quantum process and state tomography [18], quantum communication [19, 20], quantum computation [21–23], quantum annealing [24–27], ghost imaging [16, 28–30], and quantum sensor readout [31, 32]. In quantum waveform estimation, compressive sensing has been used to denoise signals [33, 34] or disambiguate frequencies in complete sets of quantum measurements [35]. Magesan *et al.* [36] proposed literal *compressive quantum sensing*, simulating the reconstruction of a neural-like signal from an incomplete set of an incomplete set of Walsh basis measurements using sparse recovery. However, the theoretical sensor, based on nitrogen vacancy (NV) centers in diamond, would decohere before a typical neural fir-

ing would complete, and no such sensor has been constructed.

Compressive quantum sensors that significantly reduce the number of required quantum measurements would make quantum waveform estimation much more practical. In particular, it would bring into view quantum sensor arrays capturing entire waveforms in a single shot. To capitalize on this promise, we need: (1) quantum sensors that stay coherent for the duration of the signal, (2) quantum sensors that measure in a basis that collects information uniformly, and (3) a post-processing algorithm that can robustly recover the signal from these measurements. Compressive sensing satisfies (3); here we demonstrate that sensors made of trapped cold atoms can satisfy (1) and (2).

Sensing electrical signals from a live *network* of *in-vitro* neurons would provide information about how nerve cells communicate with each other, and how this relates to diseases [10]. Conventionally, pulses are measured using invasive patch clamps galvanically connected to individual neurons [11]. The process perturbs neural connections and can damage cell membranes, while not scaling beyond microscopic regions of tissue. This motivates ongoing work to develop non-invasive methods which infer neuronal current waveforms from their corresponding magnetic fields. Being on the order of nanotesla at sensing range [3, 11], quantum sensors are natural candidates for magnetometers that could sense such neural signals. Quantum magnetometry of living neurons to date [2–6] has been achieved with continuous-time ensemble sensing, averaged over many nominally-identical stimulated neural responses. In contrast, we propose a projective measurement protocol, which if executed on a quantum sensing array, would plausibly sense a unique neural waveform, containing multiple firings, without averaging.

Neural waveforms are an example of *sparse* signals: those with only a small proportion of non-zero values [see Fig. 1(a)]. Consequently, information in neural waveforms is concentrated in small durations of time, and sampling in time is inherently inefficient [37]. Any uniform quantum measurement of such sparse signals will

waste quantum resources (*e.g.*, sensing time of NVs, or the limited number of projective measurements of cold atoms) by making measurements that are not very informative.

We instead reduce the number of measurements by taking non-uniform samples in a discrete sine transform (DST) [38, Eq. (37)] basis. Time sparse signals have information spread across their broad frequency spectra. Hence, one can learn all information about sparse signals using only an incomplete subset of frequency measurements [39], seemingly violating the Nyquist-Shannon sampling theorem [12, Sec. 7.1]. This is the central idea of *compressive sensing* [14, 15]. While many possible signals are consistent with a randomly chosen incomplete set of frequency measurements of a sparse signal, it is very unlikely any will be as sparse as the true signal [14, Th. 6]. One then recovers the true signal from incomplete measurements using an optimization algorithm to find the sparsest signal consistent with the measurements and a linear model of the sampling process. A hurdle for applying this to *quantum* sensing is that, to measure a frequency coefficient, the sensor would need to be coherent for the duration of the experiment. With coherence times of several seconds, trapped cold atoms are a promising candidate for such a task.

Here, we theoretically and experimentally show that cold atoms can emulate a DST-based measurement model. We then describe a recovery process that retrieves neural-like signals from an incomplete set of such measurements. Finally, we demonstrate experimental signal estimations derived from incomplete data taken from cold atoms exposed to synthesized neural-like signals.

We model our cold ^{87}Rb atom clouds as ensembles of non-interacting spin-one systems that couple to magnetic field $\mathbf{B}(t)$ via $\dot{\mathbf{H}}(t) = -\gamma \mathbf{B}(t) \cdot \hat{\mathbf{F}}$. Here $\hat{F}_{X,Y,Z}$ are spin-one hyperfine operators and γ is the appropriate gyromagnetic ratio.

We aim to measure the Fourier sine coefficient $y(f)$ of a signal $x^\natural(t)$, *i.e.*,

$$y(f) = \frac{1}{T} \int_0^T \sin(2\pi f t) x^\natural(t) dt, \quad (1)$$

for different frequencies f . To do this, we apply both a bias ω_L aligned with the signal and resonant dressing,

$$\hat{H}(t) = \omega_L \hat{F}_Z + 2\Omega \cos(\omega_{\text{rf}} t) \hat{F}_X + 2\pi x^\natural(t) \hat{F}_Z, \quad (2)$$

before readout. The system approximately measures the Fourier sine coefficient of $x^\natural(t)$ at frequency $f = \Omega/(2\pi)$, because the eigenvalues of its dressed frame (rotating at resonant ω_{rf} around Z) Hamiltonian are split by $\hbar\Omega$:

$$\hat{H}^R(t) = \Omega \hat{F}_X^R + 2\pi x^\natural(t) \hat{F}_Z \xrightarrow{\text{no signal}} \Omega \hat{F}_X^R. \quad (3)$$

(See Supplemental Material for a more technical treatment [40].) The sine component is resonant with this

splitting, resulting in transitions between dressed states at a rate proportional to $y(f)$, *i.e.*, a shift of the dressed-frame plane of Rabi-flopping shown in Fig. 1(b). Dressed state populations are mapped to lab frame \hat{F}_Z populations $N_{+,0,-}$ using a $\pi/2$ pulse [RF sequence in Fig. 1(b)], which are then measured using Stern-Gerlach absorption imaging. Starting with a superposition of dressed states, we can be linearly sensitive to small $y(f)$ via $y(f) = -\langle \hat{F}_X^R(T) \rangle / (2\pi T \hbar) = -\langle \hat{F}_Z \rangle_{\text{readout}} / (2\pi T \hbar) = (N_- - N_+)/[2\pi T (N_- + N_0 + N_+)]$. As a result, we can measure different sine coefficients by repeating experiments under this Hamiltonian while varying RF amplitude Ω .

We discretize our model for the measurement protocol in Eq. (1) as

$$y_j = \frac{1}{T} \sum_{k=1}^{K-1} \sin[2\pi(j \Delta f)(k \Delta t)] x_k^\natural \Delta t, \quad (4)$$

for $j \in \{1, 2, \dots, K-1\}$. Here the signal time series x_k^\natural starts at $k = 1$ and has length $K-1$. By choosing bandwidth as $W \stackrel{\text{def}}{=} K \Delta f = 1/(2 \Delta t)$ and sensing duration $T \stackrel{\text{def}}{=} K \Delta t = 1/(2 \Delta f)$, Eq. (4) becomes the DST [38, Eq. (37)]; *i.e.*, the matrix equation $\mathbf{y} = \mathbf{A}x^\natural$, with $A_{jk} = \sin(\pi j k / K) / K$. Compressive sensing theory roughly says that, since x^\natural is sparse, and the DCT is sensitive to all sparse signals, we can subsample our measurements and still be able to recover the signal [14, Th. 6]: *i.e.*, measure only $M < K$ components y_j of \mathbf{y} , so that now $j \in \Lambda \subset \{1, 2, \dots, K-1\}$. Equation (4) still holds, but only for $j \in \Lambda$; written $\mathbf{y}_\Lambda = \mathbf{A}_\Lambda x^\natural$, and illustrated as the matrix of sine waves of few randomly chosen frequencies in Fig. 1(b). Therefore, we know that the signal must be one of the many solutions x to the underdetermined system $\mathbf{y}_\Lambda = \mathbf{A}_\Lambda x$.

In general this is not uniquely solvable, but because x^\natural is sparse, the correct recovery, x^* , will, with high probability, be the sparsest such x [14, Th. 6]. Naïvely this is an NP-hard problem [15, Th. 2.17], but assuming that \mathbf{A}_Λ satisfies criteria involving the restricted isometry property (RIP), the sparsest solution of $\mathbf{y}_\Lambda = \mathbf{A}_\Lambda x^\natural$ will also be the solution which minimizes the ℓ_1 norm, $\|x\|_1 \stackrel{\text{def}}{=} \sum_k |x_k|$ [14, Th. 9]. These criteria translate to requirements of measuring a system-dependent minimum number of sine coefficients [15, Eq. (9.24)] and for the set of subsampled frequencies to have no structure (which is likely if it is chosen randomly [15, Th. 11.23]). In practice, our linear model [Eq. (4)] will only be approximately satisfied due to measurement noise. Hence, we relax to a problem called the *least absolute shrinkage and selection operator (LASSO)* [42, Eq. 3.14], where we find the $x \in \mathbb{R}^{K-1}$ that minimizes $\|\mathbf{A}_\Lambda x - \mathbf{y}_\Lambda\|_2^2 + \lambda \|x\|_1$, illustrated in Fig. 1(c). Here, *regularization parameter* $\lambda > 0$ [14, Sec. 8.2.2] is chosen [40] to produce the smallest error on simulated (using our open-source solver [43])

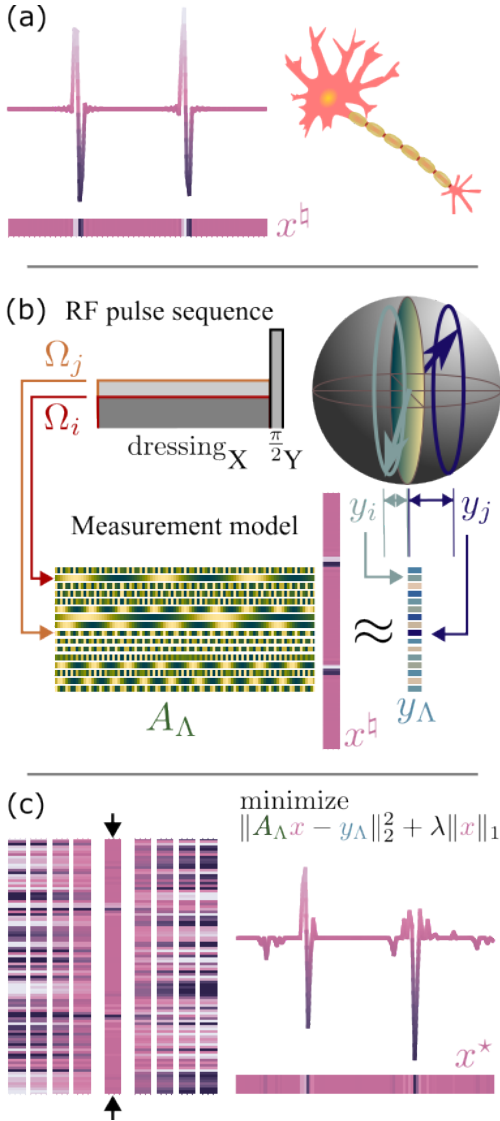


Figure 1. An overview of the protocol. (a) Trapped atoms exposed to (synthesized) neural (illustrated by phred [41] on right) magnetic signal x^h . Signal drawn as vector underneath plot. (b) Three level system (Bloch sphere on right) has Rabi frequency proportional to continuous dressing amplitude (top left). Path of Rabi flopping shifts proportional to sine coefficient y_j of x^h with frequency of Rabi flopping Ω_j . Dynamics illustrated on Bloch sphere for two possible RF amplitudes Ω_i and Ω_j (top right). Protocol modeled as an (exaggerated here) underdetermined matrix equation (bottom). Equality is approximate due to measurement noise and simplification of model. Experiment is repeated for different RF amplitudes Ω_j measuring different sine coefficients y_j . (c) FISTA searches the set of signals that fit the measurements (left) for the sparsest such signal, which it returns (right).

training data, and $\|y_\Lambda\|_2^2 \stackrel{\text{def}}{=} \sum_{j \in \Lambda} |y_j|^2$ is the ℓ_2 norm. To solve the LASSO, we implemented the *fast iterative shrinkage-thresholding algorithm (FISTA)* [44]. We chose the step-size of FISTA using the singular values of A_Λ and an estimate of the amplitude of $x(t)$.

To experimentally verify this sensing method, we applied the Hamiltonian in Eq. (2) to a dipole-trapped cloud of approximately 6×10^5 laser cooled atoms of ^{87}Rb at a temperature of order 100 nK. Here the signal $x^h(t)$ was synthesized by a coil driver, modeled as a 143 nT peak, 200 μs duration single-cycle pulse of a sine wave. This model is higher amplitude and faster than a real neural pulse (2 nT peak, 2 ms duration), so as to avoid both the sampling of AC electrical line interference, and detuning error from slow magnetic drift. However, it allows us to demonstrate a proof-of-concept and is consistent with models from other groups [5, 36]. Each term in Eq. (2) was produced by separate magnetic coils, with the bias ω_L and signal $x^h(t)$ coils being concentric, and the RF Ω coil being perpendicular. State populations $N_{+,0,-}$ were recorded using Stern-Gerlach absorption imaging of the ensemble after a readout $\pi/2$ pulse. The procedure was repeated, changing the value of Ω for each shot to record each frequency component from the incomplete set Λ . Our bias was 861 mG, giving a Larmor and radio frequency of $\omega_L \approx \omega_{\text{rf}} = 2\pi \times 603$ kHz. Our modeled neural pulse had negligible sine components above $W = 10$ kHz (consistent with Webb *et al.* [3]) which fixed our highest meaningful time resolution to be $\Delta t = 50$ μs (pulses 4 samples long). We chose an experiment duration of $T = 5$ ms ($K = 100$) in order to sense on the peak of a 20 ms-period electrical line-cycle, fixing the frequency resolution of the complete DST to $\Delta f = 100$ Hz.

We wished to compare measurements using our compressive protocol with complete measurements of both time and frequency samples. For the former, we used a separate Ramsey sequence to sample the amplitude of the signal at all of the 99 points on the time-grid. Here the second $\pi/2$ pulse was in quadrature to the first in order for the populations to be linearly sensitive to the signal (see the coherent signal case in Mouradian *et al.* [37]). The Ramsey sequences approximate capturing the field at a fixed time by sensing over a rectangular window of length 60 μs centered on the time-grid points. For the latter, we measured a complete set of 99 sine coefficients via the Hamiltonian in Eq. (2), and recovered using a complete inverse DST. Consequently, we obtained the incomplete data y_Λ for the compressive protocol by taking subsamples of the full sets of 99 sine coefficients y . Note, a *genuine* compressive sensing protocol would instead take an incomplete dataset in the first place. We provide such measurements in Supplemental Material [40].

Figure 2 compares waveform measurements of repeated one- and two-pulse signals using the Ramsey protocol, an inverse DST of the complete set of sine coefficients, and the compressive protocol using a random set of 60 of the 99 sine coefficients. The Ramsey measurements in Figs. 2(a) and (b) are unable to resolve the waveform. The recovery is overwhelmed by shot-to-shot drift of the bias magnetic field, which we later discovered was caused by suburban railway lines 2 km away. Our choice to

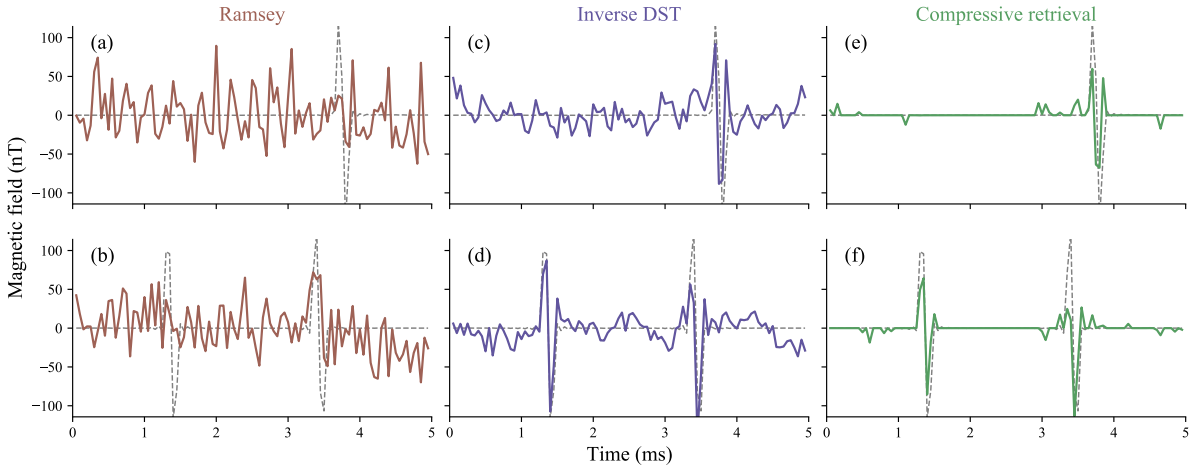


Figure 2. Neural magnetic pulses recorded using different methods. Solid signal is recovered, dashed signal is commanded to coils. (a, b) Ramsey sampling of a (a) one- and (b) two-pulse signal. Signal is not able to be recovered due to bias drift over the course of data taking. (c, d) Inverse DST using the complete set of sine coefficients recorded by the dressed atoms. (e, f) Compressive recovery using the FISTA. Here only 60 of the 99 recorded sine coefficients are used in the recovery.

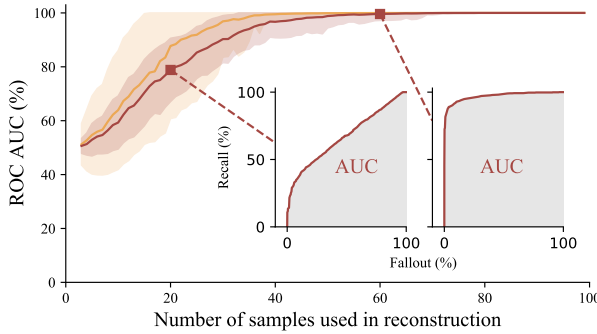


Figure 3. Finding the fewest number of samples that can be used by the compressive protocol before it fails in recovering the signal. AUC (see Supplemental Material [40]) of 100% means perfect pulse detection, 50% means random categorization. AUCs from 200 random subsets of the complete datasets were averaged to form each data point; shading shows one standard deviation either side. One-pulse traces (light orange) draw from sine coefficients used in Fig. 2(c), two-pulse traces (dark red) from Fig. 2(d). Left and right insets show ROC curves for the two-pulse signal when 20 and 60 measurements are used in the recovery respectively. ROCs are parameterized by categorization threshold. If a threshold perfectly distinguishes between pulses and noise, the ROC reaches the top left and thus encloses an area (AUC plotted in main figure) of 100%.

randomize shot order made these slow drifts appear as white noise. Another source of deviation includes the interference from the AC electrical lines. Furthermore, the square sampling window of the Ramsey measurements means that waveform estimation is susceptible to high frequency noise from surrounding instrumentation,

e.g., switching power supplies. Counterintuitively, despite only measuring short pulses, sampling for only a short duration resulted in a compromised retrieval. In contrast, recoveries from sine coefficients were able to resolve the synthesized pulses, as the DST inherently cuts out unwanted DC and high frequency coefficients. The inverse DST protocol in Figs. 2(c) and (d) are able to resolve the neural pulses more clearly than the Ramsey protocol using the same number of sensors. Additionally, despite the compressive protocol in Figs. 2(e) and (f) only taking into account 60 of the full 99 sine coefficients, it produces an even clearer signal. This is expected from the de-noising property of the LASSO [42, Fig. 6(a)].

Compressive sensing protocols have lower bounds as to how few samples can be used to recover a signal [15, Eq. (9.24)]. For our protocol, we wanted to experimentally determine this limit for our protocol and dataset. Here we compare our recovered signals to a trace of the waveform we commanded the magnetic coils with. While standard root-mean-square error is a useful metric in other contexts, we found that it had difficulty distinguishing between noisy but otherwise “successful” recoveries, and completely failed recoveries of our sparse signals. Canonical analysis of detecting signals in noise involves plotting a curve called the receiver operating characteristic (ROC); the area under the curve (AUC) [45, Sec. 7] is an appropriate metric for determining signal recovery success [40]. The AUC is 100% if a threshold can be drawn to distinguish between recovered pulses and noise, and decreases as noise and distortion drown out the signal. In Fig. 3, the compressive protocol has an AUC of over 99% when over 36 samples are used in the recovery for a signal with one pulse, over 52 for two. These echo

the known theoretical bounds of 34 and 57 for a simplified system [15, Eq. (9.24)]. We thus predict the protocol to work if 60 coefficients are used, which informed using that number for recoveries in Figs. 2(e) and (f). While a reduction in quantum resources by almost half is already enough to be useful, the theoretical model predicts even larger relative gains when measuring longer, sparser signals.

The compressive quantum sensor was able to recover neural signals in a situation where Ramsey measurements could not, while using an incomplete set of measurements. Choice of signal basis can drastically change both the fidelity, and, when undersampling, efficiency of quantum waveform estimation. This proof-of-concept demonstrates the viability of a potential quantum sensor array, where all frequency measurements are sampled by separate atom clouds parallel in space.

AT, CCB, and HT acknowledge support through Australian Government Research Training Program (RTP) scholarships. JS is the recipient of an Australian Research Council Discovery Early Career Researcher Award (project number DE210101056) funded by the Australian Government. LDT acknowledges funding from the Australian Research Council Linkage Project (project number LP200100082).

* Corresponding author; alexander.tritt@monash.edu

† Current address: Vienna Center for Quantum Science and Technology (VCQ), Faculty of Physics, University of Vienna, 1010 Vienna, Austria.

- [1] M. Tsang, H. M. Wiseman, and C. M. Caves, *Physical Review Letters* **106**, 090401 (2011).
- [2] J. F. Barry, M. J. Turner, J. M. Schloss, D. R. Glenn, Y. Song, M. D. Lukin, H. Park, and R. L. Walsworth, *Proceedings of the National Academy of Sciences* **113**, 14133 (2016).
- [3] J. L. Webb, L. Troise, N. W. Hansen, C. Olsson, A. M. Wojciechowski, J. Achard, O. Brinza, R. Staacke, M. Kieschnick, J. Meijer, A. Thielscher, J.-F. Perrier, K. Berg-Sørensen, A. Huck, and U. L. Andersen, *Scientific Reports* **11**, 2412 (2021).
- [4] L. Troise, N. W. Hansen, C. Olsson, J. L. Webb, L. Tomasevic, J. Achard, O. Brinza, R. Staacke, M. Kieschnick, J. Meijer, A. Thielscher, H. R. Siebner, K. Berg-Sørensen, J.-F. Perrier, A. Huck, and U. L. Andersen, *Laser stimulation of muscle activity with simultaneous detection using a diamond colour centre biosensor* (2021), arxiv:2112.09516 [physics.bio-ph].
- [5] J. L. Webb, L. Troise, N. W. Hansen, L. F. Frellsen, C. Osterkamp, F. Jelezko, S. Jankuhn, J. Meijer, K. Berg-Sørensen, J.-F. Perrier, A. Huck, and U. L. Andersen, *Physical Review Applied* **17**, 064051 (2022).
- [6] N. W. Hansen, J. L. Webb, L. Troise, C. Olsson, L. Tomasevic, O. Brinza, J. Achard, R. Staacke, M. Kieschnick, J. Meijer, A. Thielscher, H. R. Siebner, K. Berg-Sørensen, J.-F. Perrier, A. Huck, and U. L. Andersen, *Microscopic-scale recording of brain neuronal electrical activity us-*ing a diamond quantum sensor (2022), arxiv:2208.14068 [physics, physics:quant-ph].
- [7] N. Xu, F. Jiang, Y. Tian, J. Ye, F. Shi, H. Lv, Y. Wang, J. Wrachtrup, and J. Du, *Physical Review B* **93**, 161117 (2016).
- [8] M. Karadas, A. M. Wojciechowski, A. Huck, N. O. Dalby, U. L. Andersen, and A. Thielscher, *Scientific Reports* **8**, 4503 (2018).
- [9] M. Parashar, K. Saha, and S. Bandyopadhyay, *Communications physics* **3**, 174 (2020).
- [10] C. M. McDonald, *Physical Medicine and Rehabilitation Clinics of North America* **23**, 495 (2012).
- [11] J. Mitterdorfer and B. P. Bean, *Journal of Neuroscience* **22**, 10106 (2002).
- [12] A. V. Oppenheim and A. S. Willsky, *Signals & Systems* (Pearson Education, 1997).
- [13] D. Donoho, *IEEE Transactions on Information Theory* **52**, 1289 (2006).
- [14] N. Koep, A. Behboodi, and R. Mathar, in *Compressed Sensing and Its Applications: Third International MATHEON Conference 2017*, Applied and Numerical Harmonic Analysis, edited by H. Boche, G. Caire, R. Calderbank, G. Kutyniok, R. Mathar, and P. Petersen (Springer International Publishing, Cham, 2019) pp. 1–65.
- [15] S. Foucart and H. Rauhut, *A Mathematical Introduction to Compressive Sensing*, 2013th ed. (Birkhäuser, New York, 2013).
- [16] M. F. Duarte, M. A. Davenport, D. Takhar, J. N. Laska, T. Sun, K. F. Kelly, and R. G. Baraniuk, *IEEE Signal Processing Magazine* **25**, 83 (2008).
- [17] C. G. Graff and E. Y. Sidky, *Applied optics* **54**, C23 (2015).
- [18] Y. S. Teo and L. L. Sánchez-Soto, *International Journal of Quantum Information* **19**, 2140003 (2021).
- [19] S.-J. Ran, Z.-Z. Sun, S.-M. Fei, G. Su, and M. Lewenstein, *Physical Review Research* **2**, 033293 (2020).
- [20] K. M. Sherbert, N. Naimipour, H. Safavi, H. C. Shaw, and M. Soltanalian, *Applied Sciences* **12**, 7525 (2022).
- [21] E. Fontana, I. Rungger, R. Duncan, and C. Cirstoiu, *Efficient recovery of variational quantum algorithms landscapes using classical signal processing* (2022), arxiv:2208.05958 [quant-ph].
- [22] A. Seif, M. Hafezi, and Y.-K. Liu, *Compressed Sensing Measurement of Long-Range Correlated Noise* (2021), arxiv:2105.12589 [quant-ph].
- [23] K. Huang, D. Farfurnik, A. Seif, M. Hafezi, and Y.-K. Liu, *Random Pulse Sequences for Qubit Noise Spectroscopy* (2023), arxiv:2303.00909 [quant-ph].
- [24] R. Ayanzadeh, M. Haleem, and T. Finin, in *IGARSS 2020 - 2020 IEEE International Geoscience and Remote Sensing Symposium* (2020) pp. 3517–3520.
- [25] T. Aonishi, K. Mimura, M. Okada, and Y. Yamamoto, *Quantum Science and Technology* **7**, 035013 (2022).
- [26] R. Ayanzadeh, J. Dorband, M. Haleem, and T. Finin, in *IGARSS 2022 - 2022 IEEE International Geoscience and Remote Sensing Symposium* (2022) pp. 4911–4914.
- [27] M. D. S. H. Gunathilaka, S. Kako, Y. Inui, K. Mimura, M. Okada, Y. Yamamoto, and T. Aonishi, *Effective implementation of \$1.0\\$-Regularised Compressed Sensing with Chaotic-Amplitude-Controlled Coherent Ising Machines*, <https://arxiv.org/abs/2302.12523v1> (2023).
- [28] O. Katz, Y. Bromberg, and Y. Silberberg, *Applied Physics Letters* **95**, 131110 (2009).

[29] S. D. Johnson, P.-A. Moreau, T. Gregory, and M. J. Padgett, *Applied Physics Letters* **116**, 260504 (2020).

[30] D.-Z. Cao, S.-H. Zhang, Y. Zhao, C. Ren, J. Zhang, B. Liang, B. Sun, and K. Wang, arXiv:2108.01037 [quant-ph] (2021), arxiv:2108.01037 [quant-ph].

[31] K. Arai, C. Belthangady, H. Zhang, N. Bar-Gill, S. J. Devience, P. Cappellaro, A. Yacoby, and R. L. Walsworth, *Nature Nanotechnology* **10**, 859 (2015).

[32] D. J. Holland, M. J. Bostock, L. F. Gladden, and D. Nettispach, *Angewandte Chemie International Edition* **50**, 6548 (2011).

[33] C. Müller, X. Kong, J.-m. Cai, K. Melentijevic, A. Stacey, M. Markham, D. Twitchen, J. Isoya, S. Pezzagna, J. Meijer, J. F. Du, M. B. Plenio, B. Naydenov, L. P. McGuinness, and F. Jelezko, *Nature Communications* **5**, 4703 (2014).

[34] G. Puentes, G. Waldherr, P. Neumann, G. Balasubramanian, and J. Wrachtrup, *Scientific Reports* **4**, 4677 (2015).

[35] J. M. Boss, K. S. Cujia, J. Zopes, and C. L. Degen, *Science* **356**, 837 (2017).

[36] E. Magesan, A. Cooper, and P. Cappellaro, *Physical Review A* **88**, 062109 (2013).

[37] S. L. Mouradian, N. Glikin, E. Megidish, K.-I. Ellers, and H. Haeffner, *Physical Review A* **103**, 032419 (2021).

[38] A. Jain, *IEEE Transactions on Communications* **24**, 1023 (1976).

[39] D. L. Donoho and P. B. Stark, *SIAM Journal on Applied Mathematics* **49**, 906 (1989).

[40] See Supplemental Material at [*URL will be inserted by publisher*] for derivation of DST sensitivity, an explanation optimization setup, an explanation of the AUC performance metric, and examples of genuinely compressively sensed measurements.

[41] phreed, Single-neuron, openclipart (2006).

[42] F. Santosa and W. W. Symes, *SIAM Journal on Scientific and Statistical Computing* **7**, 1307 (1986).

[43] A. Tritt, J. Morris, J. Hochstetter, R. P. Anderson, J. Saunderson, and L. D. Turner, *Computer Physics Communications* **287**, 108701 (2023).

[44] A. Beck and M. Teboulle, *SIAM Journal on Imaging Sciences* **2**, 183 (2009).

[45] T. Fawcett, *Pattern Recognition Letters ROC Analysis in Pattern Recognition*, **27**, 861 (2006).

[46] S. Blanes, F. Casas, J. A. Oteo, and J. Ros, *Physics Reports* **470**, 151 (2009).

[47] H. F. Trotter, *Proceedings of the American Mathematical Society* **10**, 545 (1959).

[48] M. Suzuki, *Communications in Mathematical Physics* **51**, 183 (1976).

[49] S. Kay, *Fundamentals of Statistical Signal Processing, Volume II: Detection Theory, Volume 2* (Pearson Education, Englewood Cliffs, N.J, 1998).

Supplemental Material

FULL DERIVATION OF FREQUENCY SENSING PROTOCOL

The lab frame Hamiltonian of our atoms is

$$\hat{H}(t) = \omega_L \hat{F}_Z + 2\Omega \cos(\omega_{\text{rf}} t) \hat{F}_X + 2\pi x^\natural(t) \hat{F}_Z. \quad (5)$$

Moving into a frame R rotating at $\omega_{\text{rf}} = \omega_L$ (on resonance) around \hat{F}_Z , and taking the rotating wave approximation (RWA), the system has a Hamiltonian of

$$\hat{H}^R(t) = \Omega \hat{F}_X^R + 2\pi x^\natural(t) \hat{F}_Z. \quad (6)$$

We can now move into a second rotating frame RR at Ω around \hat{F}_X^R , also taking the RWA:

$$\hat{H}^{\text{RR}}(t) = -2\pi x^\natural(t) \sin(\omega_{\text{rf}} t) \hat{F}_Y^{\text{RR}} + 2\pi x^\natural(t) \cos(\omega_{\text{rf}} t) \hat{F}_Z^{\text{RR}}. \quad (7)$$

The first order Magnus expansion [46] of the time evolution operator that evolves the system for a short time step Δt in this second rotating frame is then

$$\hat{\mathcal{U}}(t + \Delta t, t) = \exp \left(-i \int_t^{t + \Delta t} \hat{H}^{\text{RR}}(t_1) dt_1 \right) \quad (8)$$

$$= \exp \left(2\pi i x^\natural(t) \sin(\Omega t) \Delta t \hat{F}_Y^{\text{RR}} - 2\pi i x^\natural(t) \cos(\Omega t) \Delta t \hat{F}_Z^{\text{RR}} \right), \quad (9)$$

to first order in Δt . Taking the Lie-Trotter [47, Th. 2] expansion [48] of this, to first order in Δt , is

$$\begin{aligned} \hat{\mathcal{U}}(t + \Delta t, t) &= \exp \left(2\pi i x^\natural(t) \sin(\Omega t) \Delta t \hat{F}_Y^{\text{RR}} \right) \\ &\quad \times \exp \left(-2\pi i x^\natural(t) \cos(\Omega t) \Delta t \hat{F}_Z^{\text{RR}} \right) \end{aligned} \quad (10)$$

We choose to start the experiment in an eigenstate ψ_{-Z} of the lab-frame spin Z operator \hat{F}_Z with an eigenvalue of $-\hbar$, as our apparatus' magnetic trap only catches atoms in this state. Then, at the start of the experiment, this initial state will also be an eigenstate of the second rotating frame spin Z operator, \hat{F}_Z^{RR} . If $|x^\natural(t)|$ stays small, then the state in RR will continue to be approximately in an eigenstate of \hat{F}_Z^{RR} throughout the experiment. We can make this assumption because the signal is both sparse (mostly zero) in the time basis, and small for realistic neural pulses. Then the \hat{F}_Z^{RR} exponential in Eq. (10) will do nothing but change the (physically meaningless) global phase of the state. Therefore, the evolution of the state is dominated by $\exp(2\pi i x^\natural(t) \sin(\Omega t) \Delta t \hat{F}_Y^{\text{RR}})$, which integrates to

$$\psi^{\text{RR}}(T) = \exp \left(i 2\pi \int_0^T x^\natural(t) \sin(\Omega t) dt \hat{F}_Y^{\text{RR}} \right) \psi_{-Z}^{\text{RR}}, \quad (11)$$

for small $x^\natural(t)$ (small angle approximation).

Thus, assuming a small signal $x^\natural(t)$, the state $\psi_{\text{RR}}(T)$ at the end of the sensing duration carries a phase proportional to the Fourier sine coefficient of $x^\natural(t)$ at a frequency of $f = \Omega/(2\pi)$. In fact, this coefficient is the expected value of \hat{F}_X^R (in both of the rotating frames). We finish the pulse sequence by applying a 20 kHz $\pi/2$ read-out pulse around \hat{F}_Y^R to rotate this expected value from \hat{F}_X^R to \hat{F}_Z . The populations of the eigenstates of \hat{F}_Z are then imaged using a Stern-Gerlach projective measurement.

TUNING OF REGULARIZATION PARAMETER

The LASSO problem needs to be tuned by the regularization parameter λ [14, Sec. 8.2.2], based on the typical noise and sparsity of measurements. We did this by recovering signals from a large set of data to optimize for which

λ produces reconstructions with the lowest average error. Since it would require a month of continuous manual data taking if real data were used, we instead used our open-source simulation python package *spinsim* [43] to generate 1000 sets of simulated experiment results. Each simulated sequence was randomly assigned 0, 1 or 2 neural pulses of amplitude 1 kHz (*i.e.*, 143 nT), each randomly placed in time. Imperfections were modelled in these experiments in the form of shot-to-shot bias drift (standard deviation of 200 Hz consistent with lab measurements) and Poisson-distributed atom shot noise (expected number of atoms exaggerated to 10^4 to also take into account photon shot noise). The error metric we chose was the average 1-norm of the difference between true and measured signals. This is the middle ground between the 0-norm [14, Sec. 2.1] which favours correct supports, and the 2-norm which favours correct amplitudes. Note that we decided *against* using area under the receiver operating characteristic (ROC) curve (AUC) (see below) as a metric for training since its landscape is very flat and therefore not informative for training. We scanned λ over 200 different values with log spacing from 100 mHz to 10 Hz, and found that value that returned the smallest error was $\lambda = 1.038$ Hz.

FULL EXPLANATION OF STATISTICAL ANALYSIS

There are three kinds of signals of interest when analysing acquired synthesized neural pulses: We have the ground truth signal x^\natural , which is a recording of the electrical signal commanded to the magnetic coils. We have the recovered signal x^* , which is the result of the compressive reconstructions or the Ramsey measurements. Finally, we have the pulse template p , which is the expected shape of each individual pulse, but it starts at $t = 0$.

The highest fidelity linear method of detecting pulse locations within a signal is by using a matched filter [49, Sec. 4.3.1]. In a matched filter, the template p is translated to all the possible starting locations in the signal, and an inner product is taken between the two via $\mu_k^\natural = \sum_j x_j^\natural p_{j+k}$. This can be written succinctly using the cross-correlation operator via $\mu^\natural = x^\natural \otimes p$, $\mu^* = x^* \otimes p$. A high value of μ_k^\natural or μ_k^* at any index corresponds to a high likelihood that a pulse is located in x^\natural or x^* respectively at time index k . We can classify locations as having a pulse or not by thresholding μ^\natural and μ^* . We obtain a ground truth classification $c^\natural = \mathcal{T}_{\|\mu\|_2^2/2}^\text{D}(\mu^\natural)$ by taking a threshold of the ground truth signal at a level of $\|\mu\|_2^2/2$. Here we define $\mathcal{T}_\Gamma^\text{D}(\mu^\natural)_k = 0$ for $\mu_k^\natural < \Gamma$, and $\mathcal{T}_\Gamma^\text{D}(\mu^\natural)_k = 1$ otherwise.

Classifications can be made of the recovered signal $c^* = \mathcal{T}_\Gamma^\text{D}(\mu^*)$ at various thresholds Γ . For each Γ , we can obtain a confusion matrix by comparing the classifications of individual locations in c^* to those in c^\natural . We have Fawcett [45, Fig. 1]

$$\# \text{ True Positives} = \text{TP} = \sum_k c_k^* c_k^\natural, \quad (12)$$

$$\# \text{ False Positives} = \text{FP} = \sum_k c_k^* (1 - c_k^\natural), \quad (13)$$

$$\# \text{ False Negatives} = \text{FN} = \sum_k (1 - c_k^*) c_k^\natural, \text{ and} \quad (14)$$

$$\# \text{ True Negatives} = \text{TN} = \sum_k (1 - c_k^*) (1 - c_k^\natural). \quad (15)$$

Two important statistics Fawcett [45, Sec. 2] can be derived from these values: recall

$$\text{rc} = \text{TP}/(\text{TP} + \text{FN}), \quad (16)$$

and fallout

$$\text{fo} = \text{FP}/(\text{FP} + \text{TN}). \quad (17)$$

Note that these are both functions of the recovery threshold Γ . The parametric curve of points (fo, rc) that Γ traces out is called the receiver operating characteristic (ROC) of the sensor [45, Sec. 4]. When $\Gamma \rightarrow -\infty$, any noise will be classified as a signal, meaning $(\text{fo}, \text{rc}) \rightarrow (1, 1)$. When $\Gamma \rightarrow \infty$, none of the true signal responses will be large enough to be classified as a signal, so $(\text{fo}, \text{rc}) \rightarrow (0, 0)$. If there is some threshold Γ^* that can completely accurately distinguish between pulses and noise, then $(\text{fo}, \text{rc}) = (0, 1)$.

The closer the ROC curve gets to this value of $(0, 1)$, the better the classifier. This can be quantified by integrating the area under the receiver operating characteristic (ROC) curve (AUC) [45, Sec. 7], auc . If the ROC curve crosses

$(0, 1)$, then it traces a square and $\text{auc} = 1$. If the classifier does no better than randomly guessing, then it traces a triangle and $\text{auc} = 1/2$. For a successful reconstruction, we would require $\text{auc} = 1$.

Figure 3 in the Letter uses AUC as a quality metric of compressive reconstructions. The insets of the figure show examples of ROCs for reconstructions made using different compression ratios.

GENUINE COMPRESSIVE MEASUREMENTS

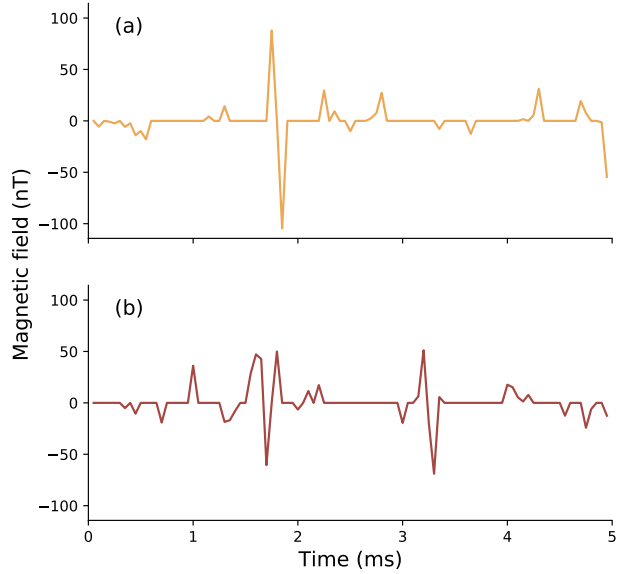


Figure 4. Reconstructions of two genuinely undersampled signals, each with only of the 60 of the possible 99 sine coefficients measured by the cold atoms.

While using the atoms to sample all sine coefficients is necessary to analyse the effectiveness of quantum compressive sensing, recording a complete dataset misses the spirit of the kind of sensor we are trying to demonstrate. For completeness, we show a compressive reconstruction of data where an incomplete measurement of sine coefficients were sensed by the atoms.

We chose 60 random frequencies out of the complete DST (*i.e.*, multiples of 100 Hz). We used the atoms to measure sine coefficients of randomly-timed synthesized pulses at these frequencies, and only these frequencies. FISTA then reconstructed the waveform based on this incomplete information.

Figure 4 shows our incomplete data sets to obtain genuinely compressed measurements. We found that though there are some noise peaks, the pulse locations can clearly be distinguished, despite being determined using incomplete information.